Evidence of structural defect enhanced room-temperature ferromagnetism in Co-doped ZnO

2007 J. Phys.: Condens. Matter 19 176229

(http://iopscience.iop.org/0953-8984/19/17/176229)

IOP PUBLISHING JOURNAL OF PHYSICS: CONDENSED MATTER

J. Phys.: Condens. Matter **19** (2007) 176229 (8pp) doi:10.1088/0953-8984/19/17/176229

Evidence of structural defect enhanced room-temperature ferromagnetism in Co-doped ZnO

C Song[1], S N Pan[1], X J Liu[1], X W Li[1], F Zeng[1], W S Yan[2], B He[2] and F Pan[1,3]

[1] Laboratory of Advanced Materials, Department of Materials Science and Engineering, Tsinghua University, Beijing 100084, People's Republic of China
[2] National Synchrotron Radiation Laboratory, University of Science and Technology of China, Hefei 230029, People's Republic of China

E-mail: panf@mail.tsinghua.edu.cn

Received 2 February 2007, in final form 5 March 2007
Published 16 April 2007
Online at stacks.iop.org/JPhysCM/19/176229

Abstract

We report experimentally that room-temperature ferromagnetism of Co-doped ZnO is strongly correlated with structural defects, and that carriers involved in carrier-mediated exchange are by nature by-products of the creation of the defects. On the other hand, the carrier concentration has pronounced influences on the absorption edge in optical transmission spectra of epitaxial Co:ZnO films, in which both a blue-shift and a red-shift are observed. Furthermore, high-temperature annealing results in evolution of the local Co structure from Co^{2+} replacing Zn^{2+} to a Co_3O_4-based phase, which most likely accounts for the transition from ferromagnetism to paramagnetism in the Co:ZnO films.

(Some figures in this article are in colour only in the electronic version)

1. Introduction

Diluted magnetic oxides (DMOs) have received the most attention as spin injector materials for spintronics [1]. Although room-temperature ferromagnetism (RTFM) has been obtained in transition-metal (TM) doped wide-bandgap semiconductors [2–6], the origin of ferromagnetism is yet to be elucidated. In the initial stage, the most studied DMO systems were characterized by carrier-mediated exchange [2, 3]. Also, some reports have shown that a second magnetic phase corresponds to the observed RTFM [7, 8]. While uniform DMO films can be both intrinsically ferromagnetic and highly insulating at room temperature, a bound magnetic polaron (BMP) model is considered as the primary mechanism [9, 10]. Additionally, there are recent predictions, not fully resolved at the present time, realizing the importance of structural defects for ferromagnetic ordering in DMOs [11–14]. For example, Kaspar *et al*

[3] Author to whom any correspondence should be addressed.

Table 1. The Co:ZnO sample identifies refer to low/high deposition rate and low/high substrate temperature (T_{sub}). The corresponding resistivity (R) and the electron concentration (n_e) are also depicted.

Sample	Rate (nm min^{-1})	T_{sub} (K)	R (Ω cm)	n_e (cm^{-3})
LH	0.9	573	$>10^3$	No Hall signal
LL	0.9	RT	5.6	2.3×10^{18}
HH	3.6	573	1.9×10^{-1}	1.5×10^{19}
HL	3.6	RT	1.7×10^{-2}	5.2×10^{19}

[13, 14] reported that, although both Co:TiO_2 films were highly resistive ($\rho > \sim$5 kΩ cm), in contrast to highly oriented but defective fast growth of Cr:TiO_2 with RTFM, the structurally superior single-crystal films that were deposited slowly with a perfect crystalline structure exhibited negligible ferromagnetism.

Structural defects are also expected to play a main role in ferromagnetic ordering in another important DMOs system, transition-metal (TM) doped ZnO [15]. However, to some extent, research on TM-doped ZnO films would be different from Co:TiO_2, primarily due to Zn loss in the deposition process [16]. Consequently, the change of electric properties with different film deposition conditions should also be taken into account when elucidating the intrinsic ferromagnetism of Co:ZnO. On the other hand, a study of the origin of RTFM not only provides an insight into the inconsistent magnetic behaviours of the TM-doped ZnO system [4, 5] but also tends to elucidate whether TM-doped ZnO can really be used in spintronics. In this paper, using complementary experiments, we study the origin of RTFM in Co-doped ZnO by clarifying the correlation of local structure, magnetic, electric and optical properties.

2. Experiment and calculation

The combination of deposition rate and substrate temperature is key in determining the crystallinity of (6 at.%) Co-doped ZnO films grown on Al_2O_3(001). $Zn_{0.94}Co_{0.06}O$ films, $\sim$105 nm thick, were deposited by rf magnetron co-sputtering at 0.9 nm min^{-1} (hereafter referred to as slow growth) and 3.6 nm min^{-1} (fast growth), 573 K and room temperature (RT), as depicted in table 1, namely samples LH, LL, HH and HL, respectively. X-ray diffraction (XRD), in both the Bragg–Bretano and pole figure geometries, were used to study the structural characteristics of the films. The surface morphologies of the samples were characterized using a field-emission scanning electron microscope (FE-SEM). X-ray absorption near-edge structure (XANES) spectra at Co K-edge and O K-edge x-ray-absorption spectroscopy (XAS) were measured to determine the valence state and local geometry in the ZnO lattice. Common background subtraction was employed in the data reduction, and the data measured in fluorescence mode were normalized and calibrated to the edge of a Co metal foil. The magnetic properties at room temperature were measured using a vibrating sample magnetometer (VSM) with magnetic fields applied parallel to the film plane. RT resistivity and Hall effect measurements were carried out using the van der Pauw geometry. Indium metal was used for the contact electrodes and the current was supplied by a dc voltage source. During the measurements, a magnetic field of $\sim$5000 Oe was applied perpendicular to the film plane.

Co K-edge XANES spectra have been calculated via the full multiple-scattering (MS) theory using the *ab initio* self-consistent FEFF 8.2 code [17] with two complementary modes: MS scattering and path analysis by examination of only the most important scattering paths. For the exchange–correlation part of the potential, we have used the energy- and position-

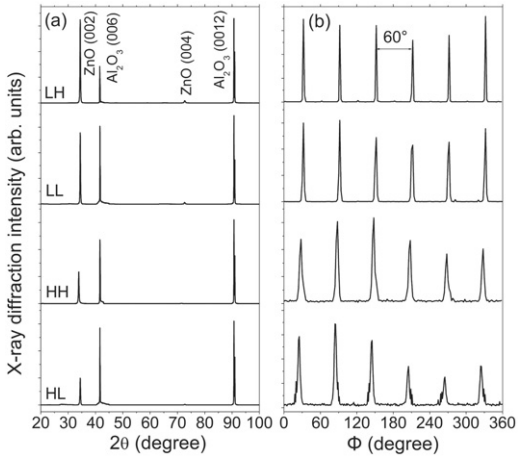

Figure 1. (a) XRD spectra of Co:ZnO films. (b) Φ scan of the {101} family peaks of Co:ZnO films.

dependent optical Hedin–Lundqvist potential with a muffin-tin radii overlap of 10% between contiguous spheres to simulate the atomic bond. These conditions have been found to produce good potentials for accurate XANES calculation of complex transition-metal oxides [17, 18].

3. Results and discussion

Figure 1(a) presents XRD patterns of four $Zn_{0.94}Co_{0.06}O$ samples, in which the two diffraction peaks are characteristic of wurtzite ZnO. The intense and sharp peaks observed suggest that the films are highly crystallized. In addition, very slow scans near the peaks of both hexagonal and cubic cobalt phases reveal no signatures of any kind of additional phases in the films. Figure 1(b) is the corresponding Φ scan of the films obtained from (101) planes, which are separated by 60°, indicating a six-fold symmetry of $Zn_{0.94}Co_{0.06}O$ in the plane [19]. Careful examination of figure 1(a) shows that ZnO(002) diffraction peak intensities become lower as the deposition rate increases and/or the substrate temperature decreases, indicating that the crystallinity of ZnO reduces with these two variables. This is demonstrated by the Φ scan, in which a comparison of the full width at half maximum (FWHM) of six-fold symmetry peak intensities shows a reduction in crystal quality and an increase of structural defects from sample LH, via samples LL and HH, to sample HL.

Co K-edge XANES and O K-edge XAS were employed to clarify the local Co structure and defect-related features in all four samples. Experimental and calculated Co K-edge XANES spectra are presented in figures 2(a) and (b), respectively. It is found that the calculated spectrum for a cluster with 77 atoms within a radius of a 6 Å sphere from the central Co atom (which replaces the central Zn in the ZnO atomic arrangement) is in reasonably good agreement with the experimental counterpart and accurately replicates three main features, marked by A_1, B_1 and C_1 in order of increasing photon energy, indicating Co^{2+} substituting for Zn^{2+}.

Concerning the details of the spectra, in figure 2(a) it is noted that the height difference between characteristic peaks B_1 and C_1 becomes larger from sample LH to HL. More interestingly, this is reproduced by the calculation displayed in figure 2(b). For example, the tetrahedrally coordinated Co photoabsorber is surrounded by a first shell composed of four oxygen atoms in sample LH, which produces a negligible height difference between B_1 and C_1. The introduction of oxygen vacancies in the first coordination results in an obvious height difference between B_1 and C_1 for samples LL and HH, which much resembles the experimental

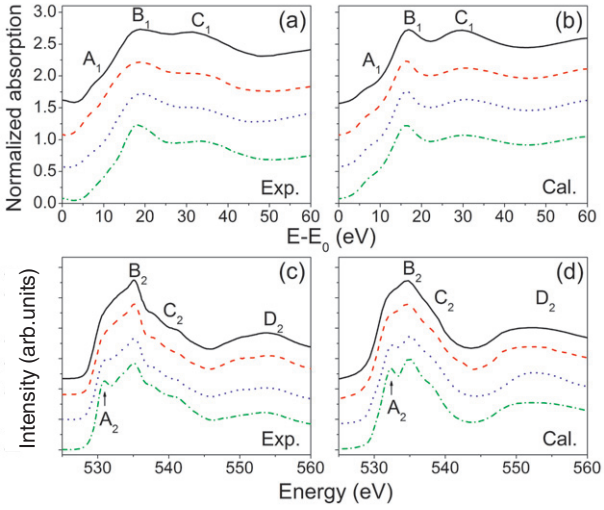

Figure 2. Experimental and calculated Co K-edge XANES spectra for Co:ZnO films are shown in (a) and (b), respectively (E_0 = 7708.8 eV). (c) and (d) show experimental and calculated O K-edge XAS for Co:ZnO films, respectively. From the upper to lower spectrum: samples LH, LL, HH and HL.

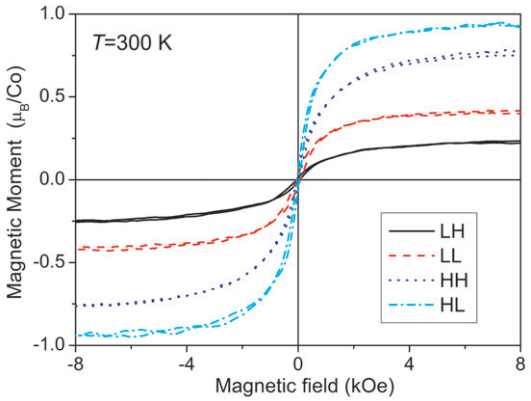

Figure 3. Typical magnetic hysteresis loops of samples LH, LL, HH and HL at room temperature.

counterpart. However, for sample HL the spectrum calculated by only introducing more oxygen vacancies to the atomic arrangement differs from the experimental observation; instead, the existence of both oxygen vacancies in the first coordination and a Zn interstitial between the first two coordinations can result in line shapes that are consistent with the experimental data. This calculation reflects less Zn loss in the deposition process for sample HL with a high deposition rate and a low substrate temperature. The situation is supported by the experimental and calculated O K-edge XAS spectra, as shown in figures 2(c) and (d), respectively. It is found that the spectrum of sample LH is similar to that of ideal stoichiometric ZnO [20], and a shoulder peak A_2 at ∼531.2 eV appears and becomes more intense from sample LL to HL, corresponding to the enhancement of defect concentrations in the Co:ZnO films according to the XAS calculation, which is also reinforced by [20]. Recalling the results of XRD, it can be considered that these point defects, i.e. oxygen vacancies and Zn interstitials, derive from a large amount of structural defects, such as edge dislocation and stacking faults [16].

Figure 3 shows the magnetization curves for the four samples, in which the average magnetic moment is obtained with respect to RT magnetic behaviour performed by a VSM and the actual Co content determined from inductively coupled plasma (ICP) atomic-emission spectra. It is useful to mention here that the diamagnetic background of the substrate has been

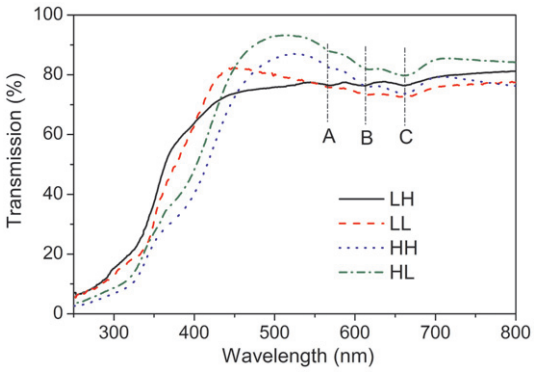

Figure 4. Room-temperature optical transmission spectra of Co:ZnO films. The spectra show characteristic absorption edges at wavelengths of about 567, 613 and 662 nm, denoted A, B and C, respectively.

subtracted from all the magnetization data shown here. For this series of films, sample LH possesses the smallest saturation magnetization of approximately 0.25 $\mu_{B/Co}$. As the film is grown at RT, i.e. sample LL, the magnetic moment enhances slightly to 0.39 $\mu_{B/Co}$. When the the film deposition rate is increased, much larger magnetic moments of ∼0.73 and ∼0.91 $\mu_{B/Co}$ are observed in samples HH and HL, respectively. A similar rate effect for Co:TiO_2 film has been reported [13, 14], whereas a higher deposition rate and subsequent subordinate crystal quality of the films lead to RTFM observed in both fast- and slow-grown samples in the present case.

RT resistivity and Hall effect measurements are performed to characterize the electric properties of the samples grown under different film deposition conditions. As exhibited by table 1, Hall effect measurements could not be performed on sample LH as the resistance was quite high. Electron concentrations (n_e) of approximately 2.3×10^{18}, 1.5×10^{19} and 5.2×10^{19} cm^{-3} are determined using the Hall effect for samples LL, HH and HL, respectively, in accordance with the suppression of the resistivity, i.e. 5.6, 1.9×10^{-1} and 1.7×10^{-2} Ω cm, respectively. Hall and resistivity measurements reveal that the conductivity of Co:ZnO films increases, from samples LH, via LL and HH to HL, which is probably due to less Zn loss in the latter samples with respect to the results of Co K-edge XANES and O K-edge XAS. As the measurements are conducted at room temperature, which for the samples is below their Curie temperature (T_c), it is worth mentioning here whether the n_e measured using the Hall effect for the present ferromagnets has true physical meaning. It is known that the Hall resistivity in ferromagnets contains two parts, e.g. the ordinary and the anomalous Hall effect [21]. In general, the anomalous Hall effect is proportional to the magnetization and is dominant at lower magnetic fields, which is usually lower than 2000 Oe [22–24]. Because the ordinary Hall effect is proportional to the applied magnetic field, it is dominant at higher magnetic field [24]. In our experiment, a comparatively high magnetic field of ∼5000 Oe is supplied during the measurements of n_e obtained from the Hall effect, as mentioned above. It is therefore thought that the ordinary Hall effect plays a dominant role in the measurements. In this case, to some extent the n_e of the present Co:ZnO ferromagnetic semiconductor can be considered as that obtained from the Hall effect in a traditional semiconductor, from a transport viewpoint. A similar method and scenario were reported by Philip *et al* [24] that the n_e were obtained from the high-field ordinary Hall effect.

RT optical transmittance spectra measurements were conducted on an ultraviolet–visible spectrophotometer, as shown in figure 4. The spectra show characteristic absorption edges at about 567, 613 and 662 nm, denoted A, B and C, respectively, resulting from the d–d transitions of the tetrahedrally coordinated Co^{2+} ions due to $^4A_2(F) \rightarrow {}^2A_1(G)$, $^4A_2(F) \rightarrow {}^4T_1(P)$ and

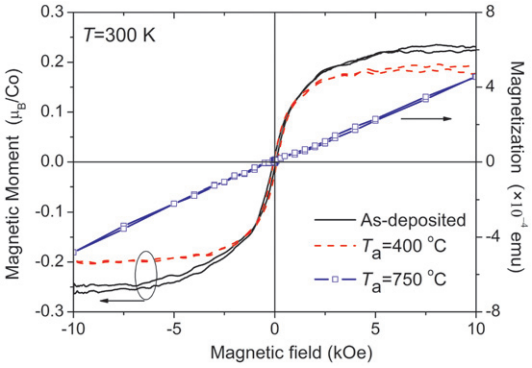

Figure 5. The magnetization of the as-deposited, 400 and 750 °C annealed sample LH.

$^4A_2(F) \rightarrow {}^2E(G)$, respectively [25]. The most interesting result here is that an apparent red-shift is observed from sample LH to LL and from sample LL to HH with increasing n_e, whereas a blue-shift can be found from sample HH to HL accompanied by a further increase in n_e. The band-gap shift is the result of two competing mechanisms: a widening (blue-shift) due to the Burstein–Moss (BM) effect [26, 27] and a band-gap-narrowing (BGN; red-shift) for the many-body effect of the electrons [28]. Our results also support the claim of Sakai *et al* [27] that the BGN shift is larger than the BM shift below an n_e of 2.8×10^{19} cm^{-3}. Interestingly, the values of n_e are lower and higher than this critical value in our case, leading to a red-shift and a blue-shift, respectively.

It is noted that magnetic behaviours as well as electric properties vary with deposition rate and substrate temperature. This phenomenon is different from Co:TiO_2 films, which show very high resistivity for both slow and fast-grown films [13, 14]. In the present case, the magnetic moment of the Co:ZnO film is seen to enhance with an increase of structural defects and n_e. Which factor is key for the enhancement of ferromagnetism? Sample LH was therefore annealed for an hour at 400 and 750 °C, respectively, in vacuum (2×10^{-6} Torr), to seek intrinsic ferromagnetism in the Co:ZnO system. The n_e of the annealed sample LH is also obtained from the RT Hall effect. After annealing at 400 °C, the n_e of sample LH increases to $\sim 2.9 \times 10^{19}$ cm^{-3}. On the other hand, the crystallinity of the Co:ZnO film is improved by the annealing, taking the microstructure characterization into account (not shown), revealing that the structural defects, e.g. edge dislocation and stacking faults, are depressed. This is consistent with the enhancement of the crystalline quality of Co:ZnO films grown at higher temperature [29]. For the magnetic measurements, it is found that the saturation magnetization reduces slightly to 0.19 μ_B/Co, as shown in figure 5, revealing that increasing n_e cannot enhance the magnetization of Co:ZnO after annealing at 400 °C. Instead, the magnetic moment per Co atom decreases with an improvement in crystallinity, indicating that the ferromagnetism of Co:ZnO is correlated with the presence of structural defects, which is analogous to the intrinsic RTFM of TM-doped TiO_2 [13, 14], and which also supports the concept of Hong *et al* [15] that the RTFM of TM-doped ZnO likely arises from structural defects.

Increasing the annealing temperature (T_a) further to 750 °C, one sees that the film does not exhibit any signature of RTFM. On the contrary, paramagnetism is unambiguously observed in figure 5, indicating that sample LH possesses paramagnetism after high-temperature (750 °C) annealing. It is important to elucidate the appearance of paramagnetism in the high-temperature annealed sample LH. The FE-SEM image of the as-deposited sample in the inset (a) of figure 6 shows just a grey background, while the 750 °C annealed sample in the inset (b) of figure 6 clearly exhibits small islands of precipitates, which are almost randomly distributed over the

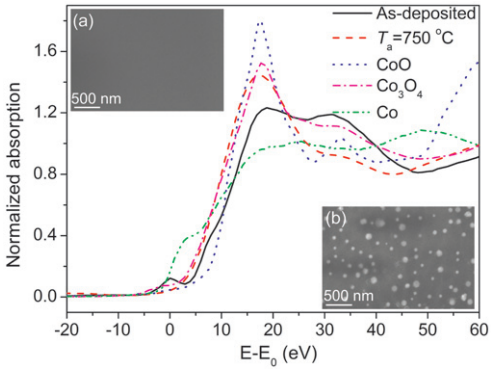

Figure 6. Co K-edge XANES spectra for the as-deposited and 750 °C annealed sample LH with Co metal, CoO and Co_3O_4 (E_0 = 7708.8 eV). FE-SEM images of the as-deposited and 750 °C annealed sample LH are shown in the insets (a) and (b), respectively.

entire range, with a size ranging from 60 to 120 nm. The XANES of the 750 °C annealed sample is different from that of the as-deposited sample. However, it closely matches that of Co_3O_4, as revealed by figure 6, characterized by a similar absorption edge, characteristic peaks, and a normalized absorption intensity. This can most probably be ascribed to Co dopants changing from Co^{2+} replacing Zn^{2+} in Co_3O_4-based compounds, which is consistent with the observations of the FE-SEM image, indicating that the sample is unstable with regard to high-temperature heat treatment. This also supports the previous observation that the RTFM of Mn:ZnO decreases via high-temperature (above 700 °C) sintering [30].

As analysed above, RTFM of Co:ZnO is sensitively dependent on structural defects, i.e. emphasizing the critical role of structural defects in governing the ferromagnetic ordering, which may also remain generally consistent with a BMP description of RTFM in Co:ZnO [13]. On the basis of the BMP model, a donor spin of the defect strongly correlating with Co^{2+} within its orbit can mediate effective interactions between them based on a Heisenberg exchange Hamiltonian. The donors then tend to shape the BMP, coupling Co^{2+} within their orbits, which try to spread out sufficiently to overlap and interact with adjacent BMP to realize magnetic ordering, resulting in RTFM [9, 10].

It should be noted that spin-polarized free carriers are subordinate in Co:ZnO, because carrier-mediated exchange is not the primary mechanism for ferromagnetic ordering. That is, Co:ZnO has few spin-polarized conduction-band free carriers, and this polarization is expected to be small. An analogous view for TM:TiO_2 has been reported by Kaspar *et al* [14]. Thus, similarly to Cr:TiO_2 [13, 14], the Co:ZnO system most likely differs from true diluted magnetic semiconductors (DMSs) such as Mn-doped GaAs [31], characterized by localized d electrons of the transition-metal ions coupling strongly with the extended sp carriers. Because the spin injection efficiency depends strongly on the free carriers' spin polarization, the small polarization means the suppression of spin injection from Co:ZnO to a traditional semiconductor. This structural defect-dependent ferromagnetism may limit Co:ZnO as a promising spin injector, and may reduce the tunnel magnetoresistance in Co:ZnO-based heterostructures, i.e. magnetic tunnel junctions (MTJs), which are under intensive study and will be published separately.

4. Conclusion

In conclusion, structural defects are of prime importance for ferromagnetic ordering in Co:ZnO. The electron concentration is not directly related to the intrinsic ferromagnetism, but it strongly affects the band shift of Co:ZnO, i.e. red-shift and blue-shift for the low and high

electron concentration regions, respectively. Moreover, the formation of the Co_3O_4-based phase afte annealing at 750 °C leads to a transition from room-temperature ferromagnetism to paramagnetism of Co:ZnO films.

Acknowledgments

The authors are grateful for financial support from the National Natural Science Foundation of China (grant nos 50325105 and 50371040). Assistance from the National Synchrotron Radiation Laboratory via the 'Innovation Plan of Education Ministry of China' is also acknowledged.

References

[1] Žutić I, Fabian J and Das Sarma S 2004 *Rev. Mod. Phys.* **76** 323
[2] Ueda K, Tabata H and Kawai T 2001 *Appl. Phys. Lett.* **79** 988
[3] Matsumoto Y, Murakami M, Shono T, Hasegawa T, Fukumura T, Kawasaki M, Ahmet P, Chikyow T, Koshihara S and Koinuma H 2001 *Science* **291** 854
[4] Prellier W, Fouchet A and Mercey B 2003 *J. Phys.: Condens. Matter* **15** R1583
[5] Janisch R, Gopal P and Spaldin N A 2005 *J. Phys.: Condens. Matter* **17** R657
[6] Liu L Q, Xiang B, Zhang X Z, Zhang Y and Yu D P 2006 *Appl. Phys. Lett.* **88** 063104
[7] Shinde S R, Ogale S B, Higgins J S, Zheng H, Millis A J, Kulkarni V N, Ramesh R, Greene R L and Venkatesan T 2004 *Phys. Rev. Lett.* **92** 166601
[8] Wei X X, Song C, Geng K W, Zeng F, He B and Pan F 2006 *J. Phys.: Condens. Matter* **18** 7471
[9] Coey J M D, Venkatesan M and Fitzgerald C B 2005 *Nat. Mater.* **4** 173
[10] Song C, Geng K W, Zeng F, Wang X B, Shen Y X, Pan F, Xie Y N, Liu T, Zhou H T and Fan Z 2006 *Phys. Rev.* B **73** 024405
[11] Bryan J D, Heald S M, Chambers S A and Gamelin D R 2004 *J. Am. Chem. Soc.* **126** 11640
[12] Hong N H, Sakai J, Poirot N and Brizé V 2006 *Phys. Rev.* B **73** 132404
[13] Kaspar T C, Heald S M, Wang C M, Bryan J D, Droubay T, Shutthanandan V, Thevuthasan S, McCready D E, Kellock A J, Gamelin D R and Chambers S A 2005 *Phys. Rev. Lett.* **95** 217203
[14] Kaspar T C, Droubay T, Shutthanandan V, Heald S M, Wang C M, McCready D E, Thevuthasan S, Bryan J D, Gamelin D R, Kellock A J, Toney M F, Hong X, Ahn C H and Chambers S A 2006 *Phys. Rev.* B **73** 155327
[15] Hong N H, Sakai J, Huong N T, Poirot N and Ruyter A 2005 *Phys. Rev.* B **72** 045336
[16] Zhang Y B, Liu Q, Sritharan T, Gan C L and Li S 2006 *Appl. Phys. Lett.* **89** 042510
[17] Ankudinov A L, Ravel B, Rehr J J and Conradson S D 1998 *Phys. Rev.* B **58** 7565
[18] Song C, Zeng F, Shen Y X, Geng K W, Xie Y N, Wu Z Y and Pan F 2006 *Phys. Rev.* B **73** 172412
[19] Prellier W, Fouchet A, Mercey B, Simon Ch and Raveau B 2003 *Appl. Phys. Lett.* **82** 3490
[20] Vaithianathan V, Lee B T, Chang C H, Asokan K and Kim S S 2006 *Appl. Phys. Lett.* **88** 112103
[21] Chien C L and Westgate C R 1980 *The Hall Effect and its Applications* (New York: Plenum)
[22] Higgins J S, Shinde S R, Ogale S B, Venkatesan T and Greene R L 2004 *Phys. Rev.* B **69** 073201
[23] Toyosaki H, Fukumura T, Yamada Y, Nakajima K, Chikyow T, Hasegawa T, Koinuma H and Kawasaki M 2004 *Nat. Mater.* **3** 221
[24] Philip J, Punnoose A, Kim B I, Reddy K M, Layne S, Holmes J O, Satpati B, Leclair P R, Santos T S and Moodera J S 2006 *Nat. Mater.* **5** 298
[25] Song C, Zeng F, Geng K W, Wang X B, Shen Y X and Pan F 2007 *J. Magn. Magn. Mater.* **309** 25
[26] Burstein E 1954 *Phys. Rev.* **93** 632
[27] Sakai K, Kakeno T, Ikari T, Shirakata S, Sakemi T, Awai K and Yamamoto T 2006 *J. Appl. Phys.* **99** 043508
[28] Schmid P E 1981 *Phys. Rev.* B **23** 5531
[29] Nielsen K, Bauer S, Lübbe M, Goennenwein S T B, Opel M, Simon J, Mader W and Gross R 2006 *Phys. Status Solidi* a **203** 3581
[30] Sharma P, Gupta A, Rao K V, Owens Frank J, Sharma R, Ahuja R, Osorio Guillen J M, Johansson B and Gehring G A 2003 *Nat. Mater.* **2** 673
[31] Macdonald A H, Schiffer P and Samarth N 2005 *Nat. Mater.* **4** 195